Hierarchical Estimation of a Dense Deformation Field for 3-D Robust Registration

P. Hellier, C. Barillot*, E. Mémin, and P. Pérez

***Abstract*—A new method for medical image registration is formulated as a minimization problem involving robust estimators. We propose an efficient hierarchical optimization framework which is both multiresolution and multigrid. An anatomical segmentation of the cortex is introduced in the adaptive partitioning of the volume on which the multigrid minimization is based. This allows to limit the estimation to the areas of interest, to accelerate the algorithm, and to refine the estimation in specified areas. At each stage of the hierarchical estimation, we refine current estimate by seeking a piecewise affine model for the incremental deformation field. The performance of this method is numerically evaluated on simulated data and its benefits and robustness are shown on a database of 18 magnetic resonance imaging scans of the head.**

***Index Terms*—Atlas matching, brain MRI, incremental optical flow, medical imaging, multigrid minimization, registration, robust estimators.**

I. Introduction

A. Context

DURING the last decade, new means of observing the human brain *in vivo* have evolved. Nowadays the users of medical images, must face not only the huge amount of data, but also the complementarity between different sets of images. For example, different magnetic resonance imaging (MRI) acquisitions are not redundant, and should not be neglected for the patient's care. Medical image registration has, thus, become a crucial issue. We distinguish several image registration applications [2].

- Registration of the same subject with the same modality. It is useful for physicians, either to follow the development of a disease, or for interventions (dynamic acquisition during the operation or its validation).
- Registration of the same subject with different modalities. This problem arises with the development of different images, either anatomical [magnetic resonance (MR), X-ray] or functional [functional MRI (fMRI), positron emission tomography (PET), electroencephalography (EEG), magnetoencephalography (MEG)]. Merging these images is desirable so that information is not excluded from the diagnostic or the therapeutic process.
- Registration of scans from different subjects. The nonlinear registration of brains from different subjects allows us to build an anatomical atlas of the cortex. Some atlases already exist [44], [49], but they appear to be inadequate, because they often lack legibility and capacity to evolve, and their interpretation is very difficult [27]. The major problem in building an atlas is the high degree of variability in the human brain. To take it into account, a nonlinear registration process is necessary. It is possible to perform automatic segmentations and to map, from one brain to the other, symbolic information such as functional activity. It has been shown [44] that we cannot assume topological equivalence between two different brains, especially for the cortical regions. Considering the same sulcus of different subjects, one may find large differences of orientation, size, and even topology (one sulcus may be interrupted or absent for instance).

B. Related Work

Medical image registration is a very active field, with recent reviews and classifications of registration procedures [36], [37], [55]. Methods are usually classified using the following criteria: the nature and the dimension [two-dimensional (2-D) or three-dimensional (3-D)] of the homologous structures to be matched, the domain of transformation (local or global), its type (rigid, affine, projective, or "free form"), the similarity measure, and the minimization scheme. We have selected a few common methods.

Because one major problem is the huge amount of data, some authors proposed methods to focus on features to be extracted and matched. These structures may be points [9], [25], curves [47], or surfaces [48], [52]. The extraction of these features is a critical issue, but the way these features are matched—and the way the registration is then computed throughout the volume—is also critical. Methods have been developed to overcome this problem: the TPS algorithm [9], spline transformations [48], the iterative closest point algorithm [47], or the "balloons" model [16].

Other registration methods are inspired by mechanical models, either elastic [1], [21], [26], or fluid [10], [14]. Fluid models allow to reach, in theory, any displacements, but these methods are highly time consuming. Christensen recently proposed [13] an interesting evolution of these methods, where the

Manuscript received April 27, 2000; revised February 5, 2001. This work was supported in part by the Brittany Country Council under a contribution to the student grant and by the GIS under Project "cognition science" (for the acquisition of the data). The Associate Editor responsible for coordinating the review of this paper and recommending its publication was J. Duncan. *Asterisk indicates corresponding author.*

P. Hellier is with the IRISA/INRIA, Campus Universitaire de Beaulieu, 35042 Rennes Cedex, France.

*C. Barillot is with the IRISA/CNRS, Project VISTA, Campus universitaire de Beaulieu, 35042 Rennes Cedex, France (e-mail: cbarillo@irisa.fr, http://www.irisa.fr/vista).

E. Mémin is with the IRISA-Université de Rennes 1, Campus Universitaire de Beaulieu, 35042 Rennes Cedex, France.

P. Pérez is with the IRISA/INRIA, Campus Universitaire de Beaulieu, 35042 Rennes Cedex, France.

Publisher Item Identifier S 0278-0062(01)03553-4.

direct deformation field and the inverse deformation field are jointly estimated to guarantee the coherence of the deformation.

Finally, some registration procedures are "voxel-based" (i.e., iconic) methods: Thirion *et al.* [45], [51] proposes the demon method; Collins [18] estimates a locally affine transformation that maximizes the cross correlation of the image gradient. Collins recently proposed [19] to introduce cortical constraints in the registration process by computing a chamfer distance between selected sulci. Musse *et al.* [42] propose a method, which is much related to the method we introduce, based on the minimization of the displaced frame difference (DFD). However, this similarity measure is highly non linear and is not robust to the acquisition artifacts of MRI. The hierarchical optimization involves β-splines, leading to a smooth deformation field that preserves the topology of the structures. That means that this field is only partially relevant, from an anatomical point of view.

C. Method

The method proposed in this paper is an extension and a complete validation of our previous work presented in [29], [30], [39], [40]. The registration problem is expressed as a motion estimation problem, which has been studied by many authors [3]–[7], [15], [31], [33], [43], [46]. Our 3-D method performs a nonlinear multimodality registration of MRI scans from different subjects. The similarity measure that we use incorporates robust estimators whose utility is twofold: on the one hand we want to limit the influence of the acquisition noise, on the other hand we want to cope with possible modifications of structures' topology.

Many tasks in computer vision may be expressed as the minimization of a cost function. Optimization is often difficult to achieve, because the cost function is nonconvex and because the optimization involves a very large number of variables. Therefore, efficient iterative multigrid (or multilevel) approaches have been developed [28], [38] and applied in motion estimation [24] and in early vision [50].

To take into account large deformations, we use a multiresolution optimization scheme. Besides, at each resolution level, we use multigrid minimization to accelerate the algorithm and improve the quality of the estimation. Within this hierarchical approach, we designed an adaptive partition of the volume to refine the estimation on the regions of interest and avoid useless efforts elsewhere. An anatomical segmentation of the cortex is introduced and used in two ways: at each resolution level, we initialize the partition as an octree subdivision based on the segmentation, and the segmentation mask is used in the subdivision criterion which controls refinement of the estimates.

II. Description of the Registration Method

A. General Formulation

The optical flow hypothesis, or brightness constancy constraint, introduced by Horn and Schunck [31], assumes that the luminance of a physical point does not vary much between the two volumes to register. It amounts to zeroing the so-called DFD

$$f(s+\mathbf{w}_s, t_1) - f(s, t_2) = 0$$

where

- s voxel of the volume;
- t_1 and t_2 indexes of the volumes (temporal indexes for a dynamic acquisition, indexes in a database for multisubject registration);
- f luminance function;
- $\mathbf{w}$ the expected 3-D displacement field.

The DFD may not be valid everywhere, because of noise and intensity inhomogeneities of MR acquisition. The robustness of the registration process with respect to acquisition artifacts will be discussed later on, in the Sections II-B and II-D.

Generally, a linear expansion of this equation is preferred: $\nabla f(s,t)\cdot\mathbf{w}_s + f_t(s,t) = 0$ where $\nabla f(s,t)$ is the spatial gradient of luminance and $f_t(s,t)$ is the voxelwise difference between the two volumes. The resulting set of undetermined equations has to be complemented with some prior on the deformation field. Using an energy-based framework (which can be viewed either from the Bayesian point of view, or from the one of the regularization theory), the registration problem may be formulated as the minimization of the following cost function:

$$U(\mathbf{w}; f) = \sum_{s\in S}[\nabla f(s,t)\cdot\mathbf{w}_s + f_t(s,t)]^2 + \alpha \sum_{\langle s,r\rangle\in\mathcal{C}} \|\mathbf{w}_s - \mathbf{w}_r\|^2 \quad (1)$$

where

- S voxel lattice;
- $\mathcal{C}$ set of neighboring pairs with respect to a given neighborhood system $\mathcal{V}$ on S ($\langle s,r\rangle \in \mathcal{C} \Leftrightarrow s \in \mathcal{V}(r)$);
- α controls the balance between the two energy terms.

The first term captures the brightness constancy constraint, thus modeling the interaction between the field (unknown variables) and the data (given variables), whereas the second term captures a simple smoothness prior. The weaknesses of this formulation are known as follows.

1) Due to the linearization, the optical flow constraint (OFC) is not valid for large displacements.
2) The OFC might not be valid in all the regions of the volume, because of the acquisition noise, intensity nonuniformity in MRI data, and occlusions.
3) The "real" field is not globally smooth and probably contains discontinuities that might not be preserved because of the quadratic smoothing.

To cope with limitations 2) and 3), we replace the quadratic cost by robust functions. To overcome limitation 1), we use a multiresolution plan and a multigrid strategy to improve the minimization at each resolution level.

We introduce a simple regularization term that makes almost no assumption on the estimated deformation field. One could imagine choosing various regularizations for the different brain tissues, but that involves specific assumptions on the "real" deformation that we did not address previously. However, the introduction of a robust estimator on the regularization term makes it possible to take into account possible discontinuities on the border of structures having different physical properties.

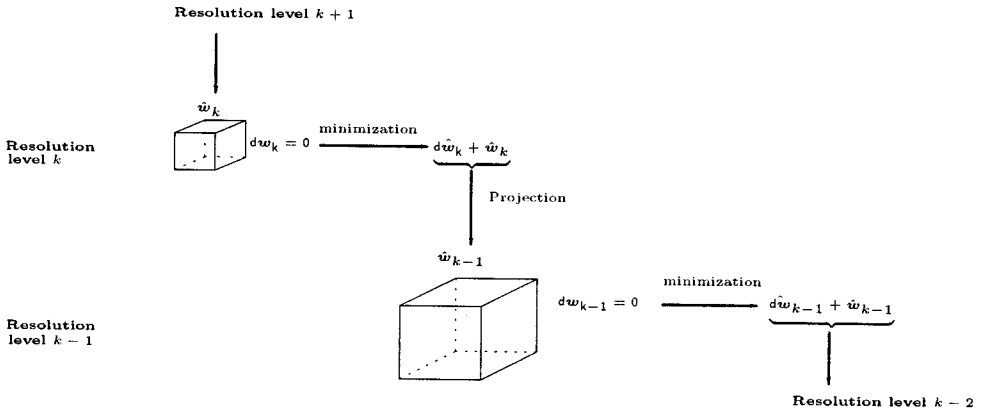

Fig. 1. Incremental estimation of the optical flow.

B. Robust Estimators

Cost function (1) does not distinguish between relevant data and inconsistent data, nor between neighboring pairs where the field is smooth and neighboring pairs where the field is discontinuous. Therefore, we introduce robust functions [32] and more precisely two robust M-estimators [8], the first one on the data term and the second one on the regularization term. We do not describe in details the properties of robust M-estimators; refer to [8] and [39] for further explanation. The cost function (1) can then be modified as

$$U(\mathbf{w};f) = \sum_{s\in S} \rho_1(\nabla f(s,t)\cdot \mathbf{w}_s + f_t(s,t)) + \alpha \sum_{\langle s,r\rangle \in \mathcal{C}} \rho_2(\|\mathbf{w}_s - \mathbf{w}_r\|). \quad (2)$$

According to some properties of robust M-estimators [8], [12], it can be shown that the minimization of U [see (1)] is equivalent to the minimization of an augmented function, noted $\overset{\star}{U}$:

$$\overset{\star}{U}(\mathbf{w},\delta,\beta;f) = \sum_{s\in S} \delta_s(\nabla f(s,t)\cdot \mathbf{w}_s + f_t(s,t))^2 + \psi_1(\delta_s) + \alpha \sum_{\langle s,r\rangle \in \mathcal{C}} \beta_{sr}\|\mathbf{w}_s - \mathbf{w}_r\|^2 + \psi_2(\beta_{sr}) \quad (3)$$

where δ_s and β_{sr} are auxiliary variables (acting as "weights") to be estimated. This cost function has the advantage to be quadratic with respect to $\mathbf{w}$. It also shows clearly that, when a discontinuity becomes larger, the contribution of the pair of neighbors is limited by the reduction of the associated weight β_{sr}. The minimizers of $\overset{\star}{U}$ with respect to the auxiliary variables are obtained in closed form [8], [12]. The overall minimization of such function consists in an alternated weights computation and quadratic minimizations (with respect to $\mathbf{w}$).

C. Multiresolution Incremental Computation of the Optical Flow

In cases of large displacements, we use a classical incremental multiresolution procedure [6], [24] (see Fig. 1). We construct a pyramid of volumes $\{f^k\}$ with successive Gaussian smoothing and subsampling in each direction [11]. For each direction $i = x, y, z$, d_i is the spatial resolution of a voxel (the spatial resolution of MR scans is approximately 1 mm, depending on the system). We perform a Gaussian filtering using the recursive implementation proposed in [23] with a standard deviation of $2 - D_i$ in direction i, in order to satisfy Nyquist's criterion. This implementation allows to perform infinite impulse response filtering at a constant computation cost.

At the coarsest level, displacements are reduced, and cost function (3) can be used because the linearization hypothesis becomes valid. For the next resolution levels, only an increment $\mathbf{dw}^k$ is estimated to refine the estimate $\hat{\mathbf{w}}^k$ obtained from the previous level. We perform the registration from resolution k_c until resolution k_f (in general $k_f = 0$). This is done using cost function (2) but with $\nabla \tilde{f}^k(s,t) \triangleq \nabla f^k(s + \hat{\mathbf{w}}_s^k, t_2)$ and $\tilde{f}_t^k(s,t) \triangleq f^k(s+\hat{\mathbf{w}}_s^k, t_2) - f^k(s,t_1)$ instead of $\nabla f^k(s,t)$ and $f_t^k(s,t)$.

To compute the spatial and temporal gradients, we construct the warped volume $f^k(s + \hat{\mathbf{w}}_s^k, t_2)$ from volume $f^k(s,t_2)$ and the deformation field $\hat{\mathbf{w}}_s^k$, using trilinear interpolation. The spatial gradient is, hence, calculated using the recursive implementation of the derivatives of the Gaussian [23]. At each voxel, we calculate the difference between the source volume and the reconstructed volume, and the result is filtered with a Gaussian to construct the temporal gradient. As previously, these quantities come from the linearization of the constancy assumption expressed for the whole displacement $\hat{\mathbf{w}}_s^k + \mathbf{dw}_s^k$. The regularization term becomes $\sum_{\langle s,r\rangle\in\mathcal{C}} \rho_2(\|\hat{\mathbf{w}}_s^k + \mathbf{dw}_s^k - \hat{\mathbf{w}}_r^k - \mathbf{dw}_r^k\|)$.

D. Multigrid Minimization Scheme

1) Motivations: The direct minimization of (3) is untractable. Some iterative procedure must be employed. Unfortunately, the propagation of information through local interaction is often very slow, leading to an extremely time-consuming algorithm. To overcome this difficulty (which is classic in computer vision when minimizing a cost function involving a large number of variables), multigrid approaches have often been designed and used in computer vision [24], [39], [50]. Multigrid minimization consists in performing the estimation through a set of nested subspaces. As the algorithm proceeds, the dimension of these subspaces increases, thus leading to a

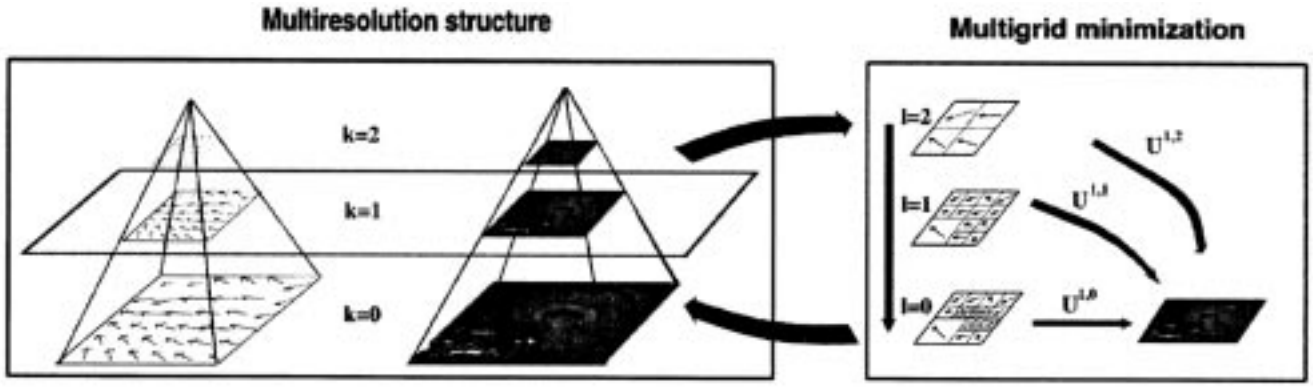

Fig. 2. Example of multiresolution/multigrid minimization. For each resolution level (a), a multigrid strategy (b) is performed. For legibility reasons, the figure is a 2-D illustration of a 3-D algorithm with volumetric data.

more accurate estimation. In practice, the multigrid minimization usually consists of choosing a set of basis functions and estimating the projection of the "real" solution on the space spanned by these basis functions.

2) Description: At each level of resolution, we use multigrid minimization (see Fig. 2) based on successive partitions of the initial volume [39]. At each resolution level k, and at each grid level ℓ, corresponding to a partition of cubes, we estimate an incremental deformation field $\mathsf{dw}^{k,\ell}$ that refines the estimate $\hat{\mathbf{w}}^k$, obtained from the previous resolution levels. This minimization strategy, where the starting point is provided by the previous result—which we expect to be a rough estimate of the desired solution—, improves the quality and the convergence rate compared with standard iterative solvers (such as Gauss–Seidel).

At grid level $\ell, \Xi_\ell = \{\Xi_n, n = 1 \dots N_\ell\}$ is the partition of the volume B into N_ℓ cubes Ξ_n. At each grid level ℓ corresponds a deformation increment $\mathsf{T}_{k,\ell}$ that is defined as follows: A 12-dimensional parametric increment deformation field is estimated on each cube Ξ_n, hence, the total increment deformation field $\mathsf{dw}^{k,\ell}$ is piecewise affine. At the beginning of each grid level, we construct a reconstructed volume with the target volume $f^k(s, t_2)$ and the field estimated previously (see Section II-C). We compute the spatial and temporal gradients at the beginning of each grid level and the increment deformation field $\mathsf{dw}^{k,\ell}$ is initialized to zero. The final deformation field is, hence, the sum of all the increments estimated at each grid level, thus expressing the hierarchical decomposition of the field.

Contrary to block-matching algorithms, we model the interaction between the cubes (see Section II-E) of the partition, so that there is no "block-effects" in the estimation. At each resolution level k, we perform the registration from grid level ℓ_c until grid level ℓ_f. Depending on the application, it may be useless to compute the estimation until the finest grid level, i.e., $\ell_f = 0$. We will evaluate this fact later on (see Section III-A).

3) Adaptive Partition: To initialize the partition at the coarsest grid level ℓ_c, we consider a segmentation of the brain obtained by morphological operators. After a threshold and an erosion of the initial volume, a region growing process is performed from a manually chosen starting point. A dilatation operation produces a binary segmentation. At grid level ℓ_c, the partition is initialized by a single cube of the volume size.

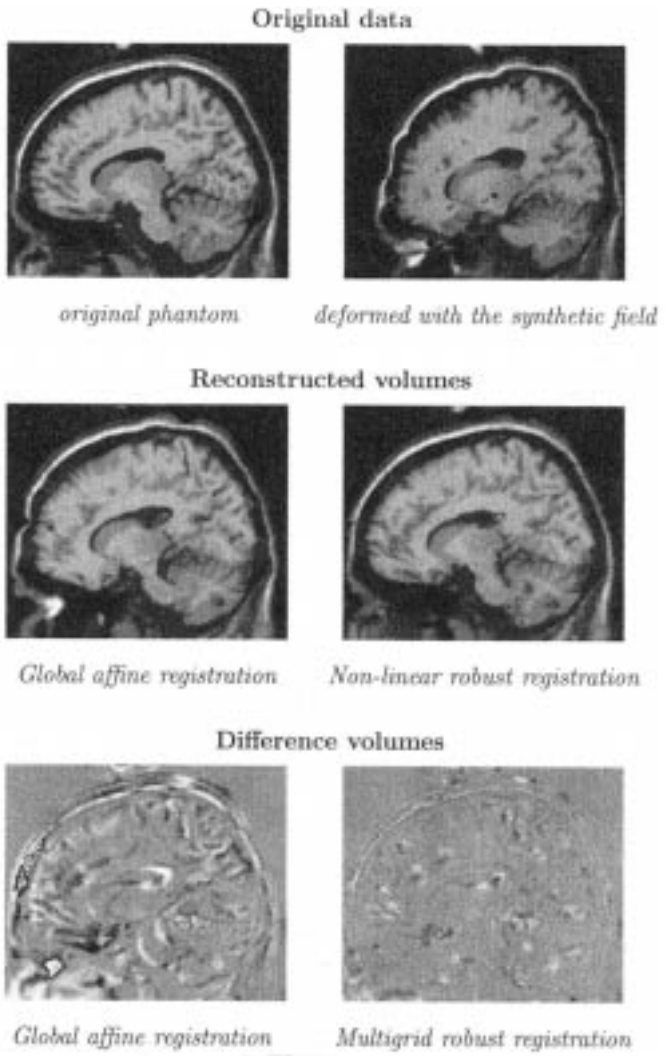

Fig. 3. Results of the registration process on simulated data. The 3-D MRI phantom has been deformed on the top of the figure. In the middle, the reconstructed volumes are shown and must be compared with the initial volume to evaluate the quality of the registration. On the bottom, the difference volumes show the benefits of nonlinear registration.

TABLE I
OBJECTIVE MEASURES OF THE QUALITY OF THE REGISTRATION ON SIMULATED DATA. SPECIFICITY, SENSITIVITY, AND TOTAL PERFORMANCE MEASURES ARE GIVEN FOR THREE LEVELS OF NOISE AND TWO REGISTRATION METHODS

		noise 0% inhomogeneity 0%			noise 3% inhomogeneity 20%			noise 9% inhomogeneity 40%		
		Target volume	Grey matter	White matter	Target volume	Grey matter	White matter	Target volume	Grey matter	White matter
	Computation time	10′			10′			10′		
	MSE	964.63	2679.49	1751.41	1104.22	3305.50	2171.13	2005.14	6933.05	5031.49
Global	sensitivity		93.78%	91.19%		93.26%	89.01%		83.21%	77.33%
Affine	specificity		93.16%	93.72%		91.69%	92.48%		83.19%	85.42%
	total performance		93.27%	93.41%		91.97%	92.06%		83.19%	85.42%
	Computation time	55′			61′			76′		
	MSE	138.57	1383.46	886.53	233.23	1534.48	970.42	667.88	3186.49	1463.87
Robust	sensitivity		97.83%	97.35%		97.09%	96.36%		95.50%	93.27%
Multigrid	specificity		94.28%	94.35%		94.76%	94.90%		90.73%	93.67%
	total performance		94.91%	94.71%		95.35%	95.03%		91.50%	93.80%

The registration processes are performed until resolution 0 (voxel size 1 mm^3). We manage to recover up to 93% of the deformation even in presence of important noise (9%) and image intensity inhomogeneity (40%). The cpu times are given for an Ultra Sparc at 333 MHz.

We iteratively divide each cube as long as it intersects the segmentation mask and as long as its size is superior to $2^{3\ell_c}$. We finally obtain an octree partition which is anatomically relevant.

When we change from grid level, each cube is adaptively divided. The subdivision criterion depends first on the segmentation mask (we seek maximum precision on the cortex), but it also depends on the local distribution of the variable δ_s [see (3)]. More precisely, a cube is divided if it intersects the segmentation mask or if the mean of δ_s on the cube is below a given threshold. In fact, δ_s indicates the correspondence between the data and the estimated deformation field at voxel s. Therefore, this criterion combines an indicator of the confidence about the estimation with a relevant anatomical information.

E. Parametric Model

We now introduce the deformation model that is used. We chose to consider an affine 12-parameter model on each cube of the partition, commonly used in computer vision but rarely used in medical imaging. If a cube contains less than 12 voxels, we only estimate a rigid six-parameter model, and for cubes that contain less than six voxels, we estimate a translational displacement field. As we have an adaptive partition, all the cubes of a given grid level might not have the same size. Therefore, we may have different parametric models, adapted to the partition.

At a given resolution level k and grid level $\ell, \Xi_{k,\ell} = \{\Xi_n, n = 1 \dots N_{k,\ell}\}$ is the partition of the volume into $N_{k,\ell}$ cubes Ξ_n. On each cube Ξ_n, we estimate an affine displacement defined by the parametric vector $\Theta_n^{k,\ell} : \forall s = (x,y,z) \in \Xi_n, \mathbf{dw}_s = P_s \Theta_n^{k,\ell}$, with

$$P_s = \begin{pmatrix} 1 & x & y & z & 0 & 0 & 0 & 0 & 0 & 0 & 0 & 0 \\ 0 & 0 & 0 & 0 & 1 & x & y & z & 0 & 0 & 0 & 0 \\ 0 & 0 & 0 & 0 & 0 & 0 & 0 & 0 & 1 & x & y & z \end{pmatrix}.$$

A neighborhood system $V^{k,\ell}$ on the partition $\Xi_{k,\ell}$ derives naturally from $\mathcal{V}$ (see Section II-A).

$\forall n, m \in \{1 \dots N_{k,\ell}\}, m \in V^{k,\ell}(n) \Leftrightarrow \exists s \in \Xi_n, \exists r \in \Xi_m \backslash r \in \mathcal{V}(s)$. $\mathcal{C}$ being the set of neighboring pairs on S^k, we must now distinguish between two types of such pairs: the pairs inside one cube and the pairs between two cubes

$$\begin{aligned} &\forall n \in \{1 \dots N_{k,\ell}\}, \quad \langle s, r \rangle \in \mathcal{C}_n^\ell \Leftrightarrow s \in \Xi_n, \\ &\quad r \in \Xi_n \quad \text{and} \quad r \in \mathcal{V}(s). \\ &\forall n \in \{1 \dots N_{k,\ell}\}, \quad \forall m \in V^\ell(n), \\ &\langle s, r \rangle \in \mathcal{C}_{nm}^\ell \Leftrightarrow m \in V^l(n), \\ &\quad s \in \Xi_n, r \in \Xi_m \quad \text{and} \quad r \in \mathcal{V}(s). \end{aligned}$$

For conciseness, we drop the resolution index k. With this notation, the cost function (3) becomes (4), as shown at the bottom of the next page.

Considering the auxiliary variables of the robust estimators as fixed, one can easily differentiate the cost function (4) with respect to any Θ_n^ℓ and get a linear system to be solved. We use a Gauss–Seidel method to solve it for its implementation simplicity. However, any iterative solver could be used (solvers such as conjugate gradient with an adapted preconditioning would

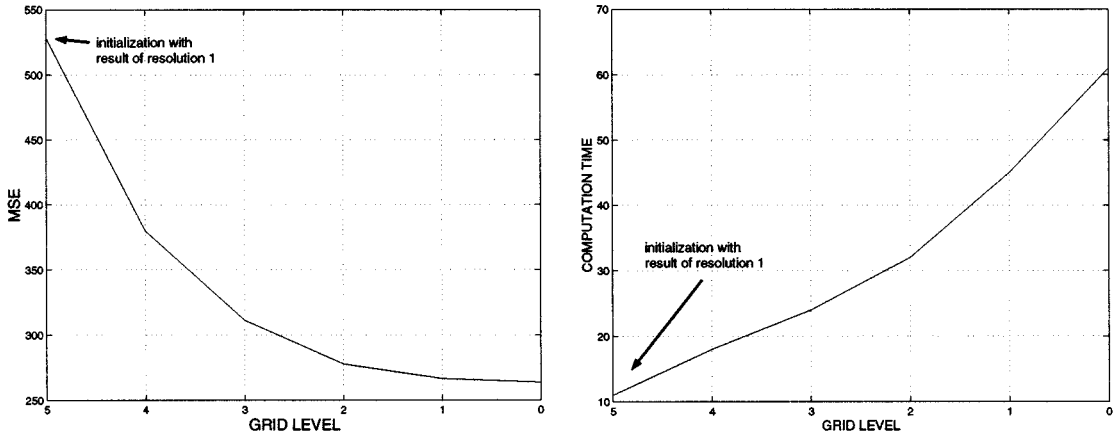

Fig. 4. Evolution of the mean square error (mse) with respect to the grid level (at finest resolution 1 mm) and computation time needed to perform the registration until a given grid level. We observe that the mse decreases significantly at coarsest grid level, whereas at finest grid level it continues to decrease, but less rapidly. At the same time, the computation time increases continuously. If we look at the difference between grid level 2 (the smallest cubes are of size $2^2 \times 2^2 \times 2^2$ and the incremental deformation field is affine on each cube) and grid level 0 (the smallest cubes are reduced to a voxel and the incremental deformation field is translational for the smallest cubes), the computation time increases of 100%, whereas the mse variation is only 5.3%. That suggests that, depending on the application, the user can make a compromise between the accuracy of the registration and the computation time if the resources are limited.

be for example more efficient). In turn, when the deformation field is "frozen," the weights are obtained in a closed form [8], [12]. The minimization may, therefore, be naturally handled as an alternated minimization (estimation of Θ_n^ℓ and computation of the auxiliary variables). Contrary to other methods (minmax problem like the demons' algorithm for instance), that kind of minimization strategy is guaranteed to converge [12], [22], [41] (i.e., to converge toward a local minimum from any initialization).

Moreover, the multigrid minimization makes the method invariant to intensity inhomogeneities that are piecewise constant. As a matter of fact, if the intensity inhomogeneity is constant on a cube, the restriction of the DFD on that cube is modified by adding a constant. As a consequence, minimizing the cost function (4) gives the same estimate, whenever the cost at the optimum is zero or a constant (see Section III-A1 for an illustration on that issue).

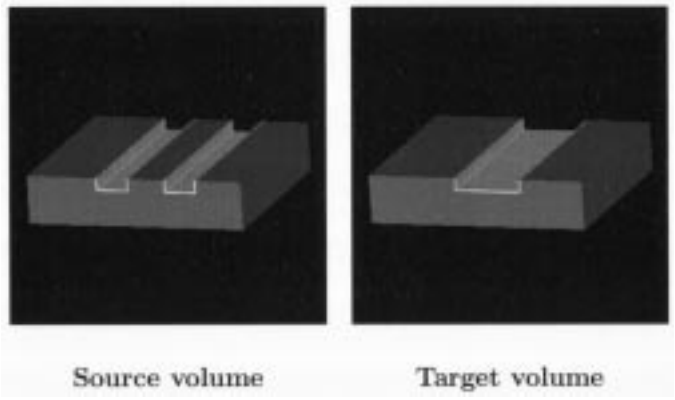

Fig. 5. Synthetic data to validate the link between robust estimator on the regularization term and local changes of topology.

III. Results

A. Experiments on Simulated Data

1) Evaluation on the MNI Phantom: To evaluate the global registration method, we use the simulated data provided by the MNI (Brainweb: http://www.bic.mni.mcgill.ca/brainweb) [17]. Data have been collected with three levels of noise and inhomogeneity. We design a synthetic deformation field made up of a global affine field with large deformations combined with local stochastic perturbations. We do not try to build a "realistic" field, but rather a field with the following properties: large de-

$$\begin{aligned}\overset{\star}{U}^{\ell}(\Theta^\ell,\delta^\ell,\beta^\ell;\mathbf{w},f^\ell) = &\sum_{n=1}^{N_\ell}\sum_{s\in\Xi_n}\delta_s^\ell\left[\nabla\tilde{f}_s^T P_s\Theta_n^\ell+\tilde{f}_t(s,t)\right]^2+\psi_1\left(\delta_s^\ell\right)\\ &+\alpha\sum_{n=1}^{N_\ell}\left[\sum_{m\in V^\ell(n)}\sum_{\langle s,r\rangle\in\mathcal{C}_{nm}^\ell}\beta_{sr}^\ell\left\|\left(\mathbf{w}_s+P_s\Theta_n^\ell\right)-\left(\mathbf{w}_r+P_r\Theta_m^\ell\right)\right\|^2+\psi_2\left(\beta_{sr}^\ell\right)\right]\\ &+\alpha\sum_{n=1}^{N_\ell}\left[\sum_{\langle s,r\rangle\in\mathcal{C}_n^\ell}\beta_{sr}^\ell\left\|\left(\mathbf{w}_s+P_s\Theta_n^\ell\right)-\left(\mathbf{w}_r+P_r\Theta_n^\ell\right)\right\|^2+\psi_2\left(\beta_{sr}^\ell\right)\right]. \qquad (4)\end{aligned}$$

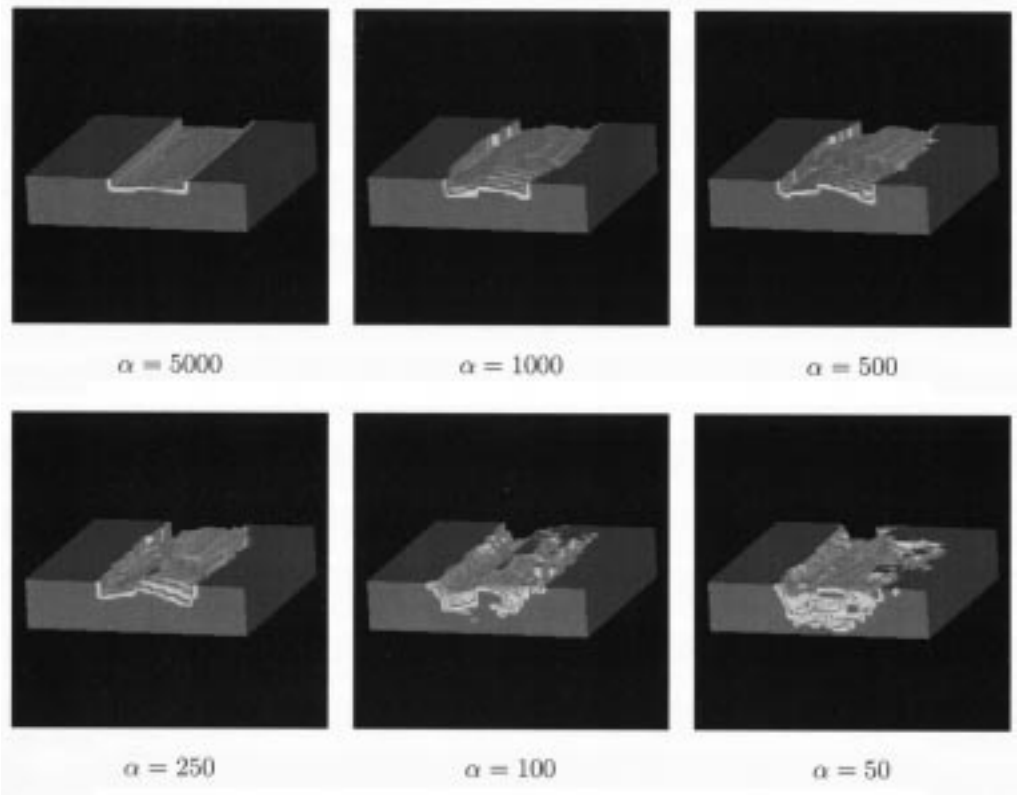

Fig. 6. Results of the registration without robust estimator. The different volumes correspond to different values of the parameter α, and must be compared to the source volume.

formations and local perturbations that modify the topology of the structures, in order to validate the basic hypothesis of our work. The "local" field is generated from 2000 voxels which are randomly picked in the volume. For each voxel, each of the three components of the deformation is the realization of a Gaussian random variable of standard deviation 120 mm. We then perform Gaussian smoothing with a small average deviation in order to propagate this perturbation to a local neighborhood while preserving discontinuities. The volumes and the results are shown in Fig. 3. We compare the multigrid method with a global affine registration method, in which a 12-parameter deformation is estimated for the entire volume.

To asses the quality of the registration, we compute the mean square error (mse)[1] which is an indicator of the quality of the registration. However, it would be unfair to evaluate the registration only with a measure that is the underlying driving force of the estimation. Therefore, as we have the binary classification of the phantom, we can also assess the quality of the registration based on the overlap of two volumes: the first volume is the initial classification, i.e., a gold standard (grey matter/white matter), the second volume is the deformed classification, registered with the estimated deformation field. We then measure overlapping ratios such as the sensitivity, the specificity, and the total performance [54]. Results are presented on Table I. Despite the use of binary classes, the resulting measures that we obtain are very satisfactory. Particularly, the robustness of the method is demonstrated in critical conditions (9% noise and 40% inhomogeneity), which are far tougher than in any realistic acquisition.

[1]mse $= (1/N)\sum_{i=1}^{i=N}(I_1(i) - I_2(i))^2$, where I_1 and I_2 are the volumes to compare, and N is the number of voxels.

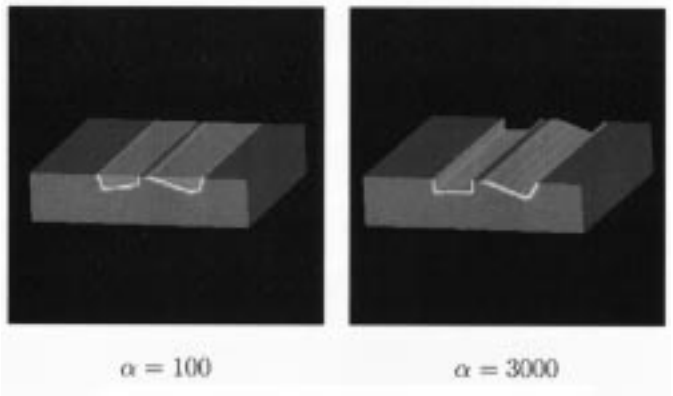

Fig. 7. Results of the registration with a robust estimator on the regularization term. The reconstructed volumes must be compared to the source volume. We can handle with local topology changes, while preserving the global smoothness of the solution.

The numerical evaluation also allows to study the sensitivity of the algorithm with respect to the parameters of the algorithm, i.e., parameters of the robust estimators. We have two parameters to fix, σ_1 and σ_2. σ_1 corresponds to the hyperparameter of robust function ρ_1, associated with the similarity term, while σ_2 corresponds to the hyperparameter of robust function ρ_2 associated with the regularization term. We made the parameters σ_1 and σ_2 vary in a cube of size $[1.0e^4, 1.0e^5] \times [1, 20]$ with step respectively of $1.0e^4$ and 1 (which means that we performed the registration with 200 different sets of parameters), and we ob-

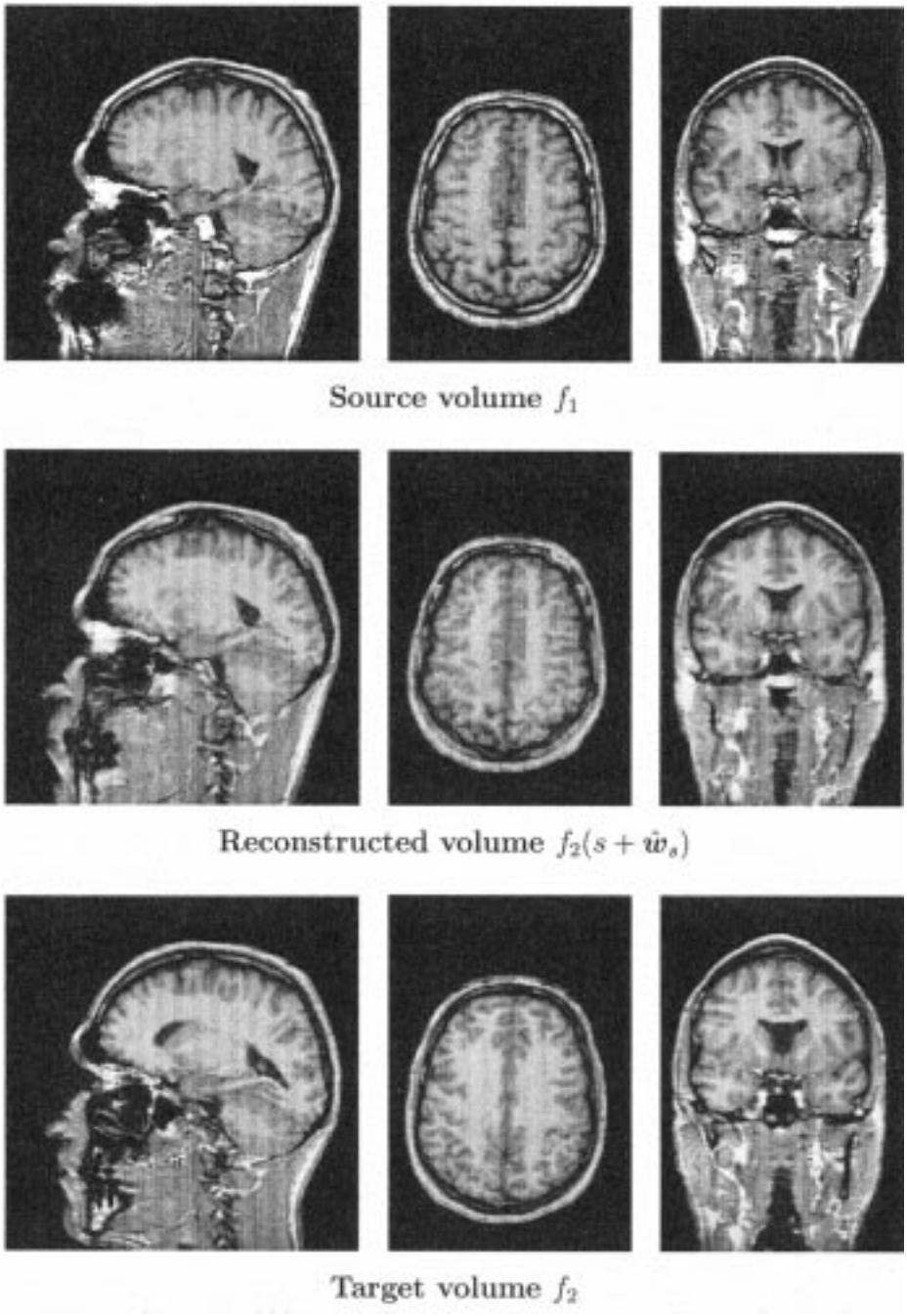

Fig. 8. Final 3-D results of the registration on real data. The volumes are T1-MRI acquisitions of two different subjects. The reconstructed volume is computed by trilinear interpolation with the target volume and the final dense displacement field. In order to evaluate the quality of the registration, we must, therefore, compare the source volume and the reconstructed volume.

serve that the final result (the mse between the source volume and the reconstructed volume) varies less than 5% of the nominal mse. This indicates that the sensitivity of algorithm with respect to these two parameters is very low.

For simulated data, mse is a direct measure of the quality of the registration. Therefore, we can evaluate also the influence of ℓ_f (see Section II-D3) on the computation time and on the accuracy of the registration. Fig. 4 shows the evolution of the mse with respect to the grid level (at finest resolution 1 mm) and also shows the computation time needed to perform the registration until a given grid level. We observe that the mse decreases significantly at coarsest grid level, whereas at finest grid level it continues to decrease, but less rapidly. At the same time, the computation time increases continuously. If we look at the difference between grid level[2] 2 and grid level[3] 0, the computation time increases of 100%, whereas the mse variation is only 5.3%. That suggests that, depending on the application, the user compromise between the accuracy of the registration and the com-

[2]The smallest cubes are of size $2^2 \times 2^2 \times 2^2$ and the increment deformation field is affine on each cube.

[3]The smallest cubes are reduced to a voxel and the increment deformation field is translational for the smallest cubes.

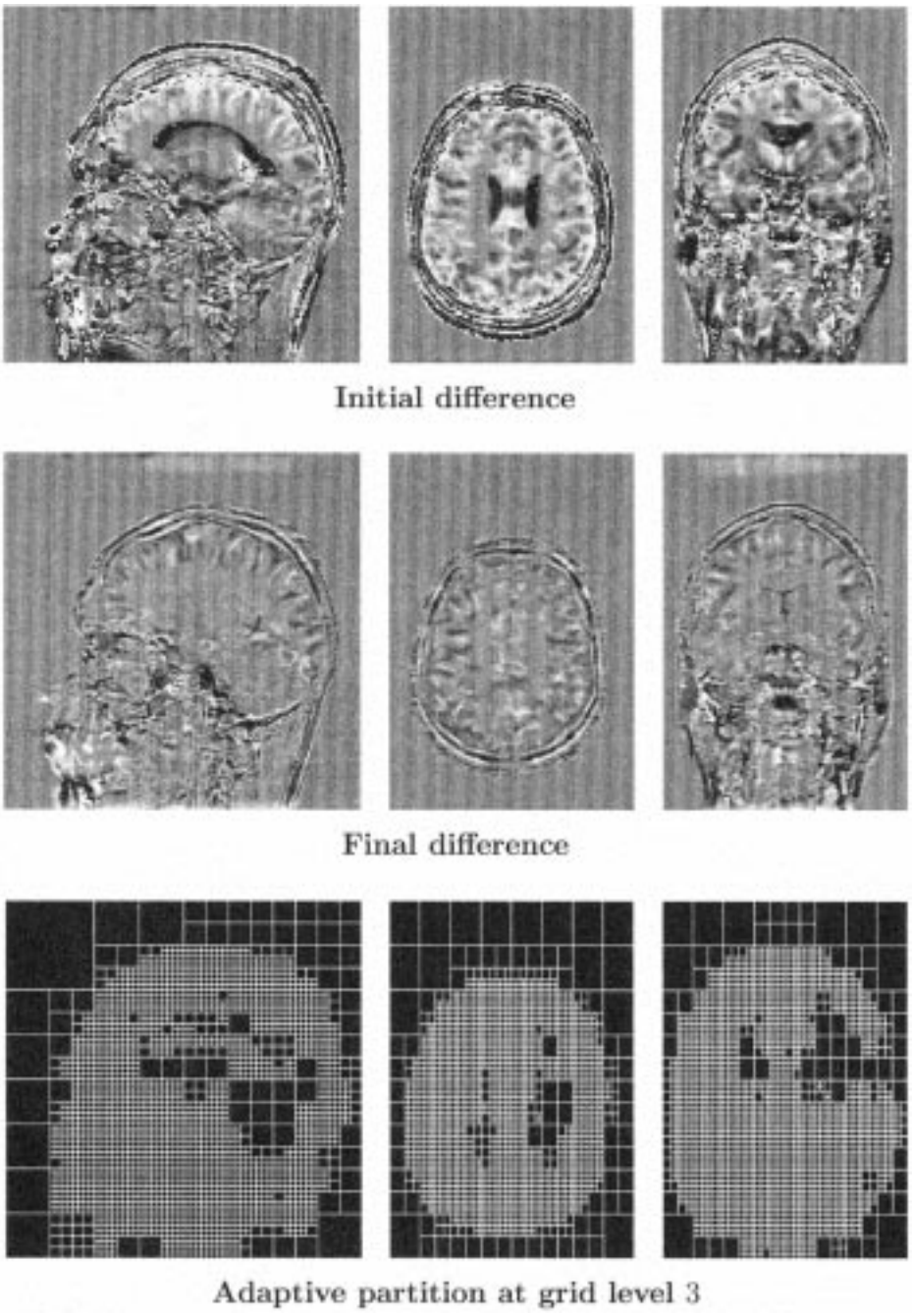

Fig. 9. Final 3-D results of the registration on real data. Top: Difference before registration. Middle: Difference after registration. Bottom: Adaptive partition at grid level 3. The difference volumes must be interpreted carefully, since we havethe superposition of two errors: the first one is the registration error which comes from the anatomical variability that we could not apprehend. The second error is due to the difference of acquisition of the two volumes, which makes the two original histograms of the two volumes different.

putation time if its resources are limited. In our case, we find that $\ell_f = 1$ (the smallest cubes are of size $2 \times 2 \times 2$ and the allowed deformation is rigid on the smallest cube) is generally a good compromise.

2) Importance of Robust Estimator: We have introduced robust estimators in the registration process, to allow local discontinuities of the deformation field to occur. To verify the direct link between the introduction of a robust function and the possibility of local change in the topology of the structures on simulated data, we constructed two volumes (see Fig. 5) to be registered, with a local modification of the topology. The volumes are composed of two homogenous classes, each one being defined by a unique grey level. With these two volumes, we obviously face the aperture problem, which is classic in the optical flow literature.

We first register the two volumes without any robust estimator. Results are presented in Fig. 6. The reconstructed volumes are computed with the target volume and the estimated deformation field with trilinear interpolation. One must, therefore, compare the reconstructed volume and the source volume to assess the quality of the registration. The different volumes shown in Fig. 6 correspond to different values of the param-

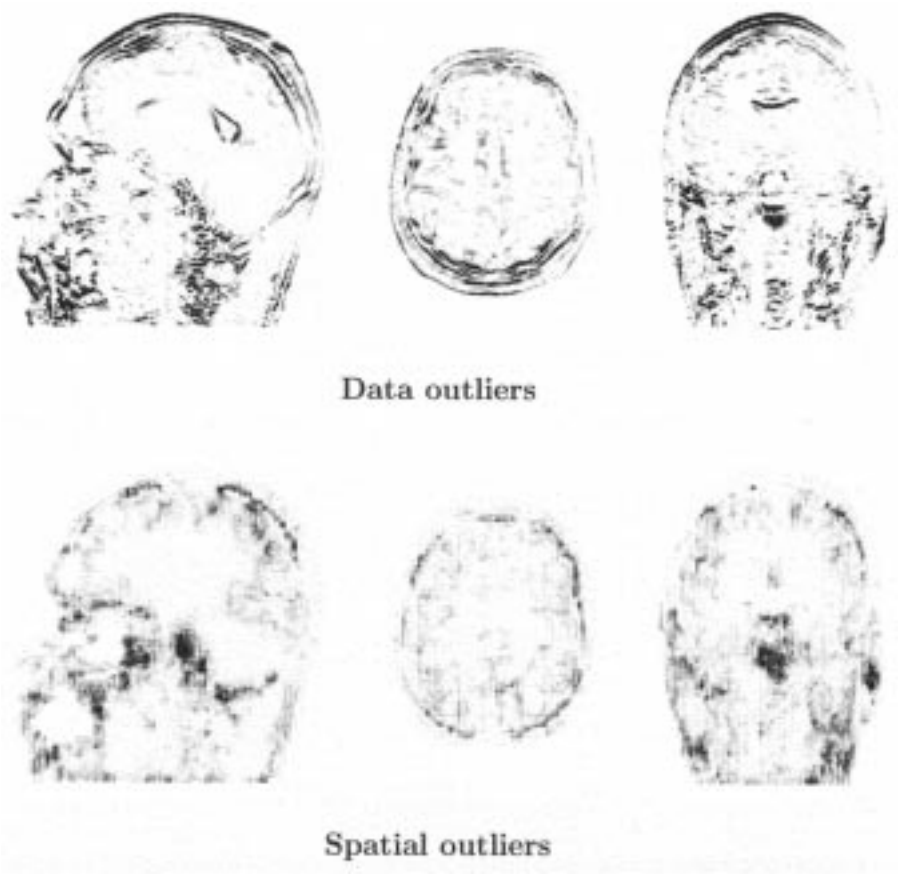

Fig. 10. Final 3-D results of the registration on real data. Top: data outlier map. Middle: spatial outlier map. Looking at the spatial outlier term, we observe that dark regions are located in the cortex. Dark areas shows that the importance of the regularization term is reduced, and discontinuities can appear. The fact that discontinuities appear in the cortex is significant because we know that inter-subject variability is very high on the cortex.

eter α. This parameter balances the importance of the similarity term and the regularization term. When this parameter is high, the solution is smooth but the topology is not modified. When α decreases, the solution is not smooth, the aperture problem is obvious, whereas the topology is not correctly modified.

We then perform the robust multigrid registration process, with a robust function only on the regularization term. Results are presented in Fig. 7, with two "extreme" values of the parameter α. In that case, the modification of the topology is possible, while preserving the global smoothness of the solution. However, the aperture problem is still present on the tubular structure on the right. This experiment makes it possible to verify the link between the introduction of a robust estimator on the regularization term and the possibility to handle local change of topology. In addition, the robust registration process appears to be also more robust with respect to the parameter α, because the results of the registration are very similar, when α varies in a range of $[100, 3000]$.

B. Experiment on 2 Subjects

Results of the 3-D method are presented in Figs. 8, 9, and 10. Two 3-D MRI-T1 volumes of two different subjects are registered. The source volume, the target volume and the reconstructed volume are presented oin Fig. 8. The reconstructed volume $f_2(s + \hat{\mathbf{w}}_s)$ is computed with the target volume f_2 and the final displacement field $\hat{\mathbf{w}}$ by the way of a trilinear interpolation. To assess the quality of the registration, one must compare the source volume with the reconstructed volume.

We also present the volumes of difference, before and after registration on Fig. 9. On the same figure, the adaptive partition at grid level 3 is also presented (we do not present further grid levels for readability reasons). The difference volumes must be interpreted carefully, since we ghave the superposition of two errors: the first one is the registration error which comes from the anatomical variability that we could not apprehend. The second error is due to the difference of acquisition of the two volumes, which makes the histograms of the source and target volumes different.

In Fig. 10, the outliers are drawn, i.e., the data outliers map (variable δ_s) and the spatial outlier map (for each point s, we compute the mean of variable β_{sr} with respect to $r \in \mathcal{V}(s)$). Looking at the data outliers map, the dark points represent areas where the optical flow hypothesis is inadequate, because of occlusions for instance (see the jaw in Fig. 10). For these points, the regularization term overwhelms the similarity term. Looking at the spatial outlier term, we observe that dark regions are located in the cortex. At that locations, the importance of the regularization term is reduced, and discontinuities can appear. The fact that discontinuities appear in the cortex is significant because we know that inter-subject variability is very high on the cortex.

The 3-D deformation field is presented in Fig. 11. The vector field is subsampled in order to be easier to look at, and we also

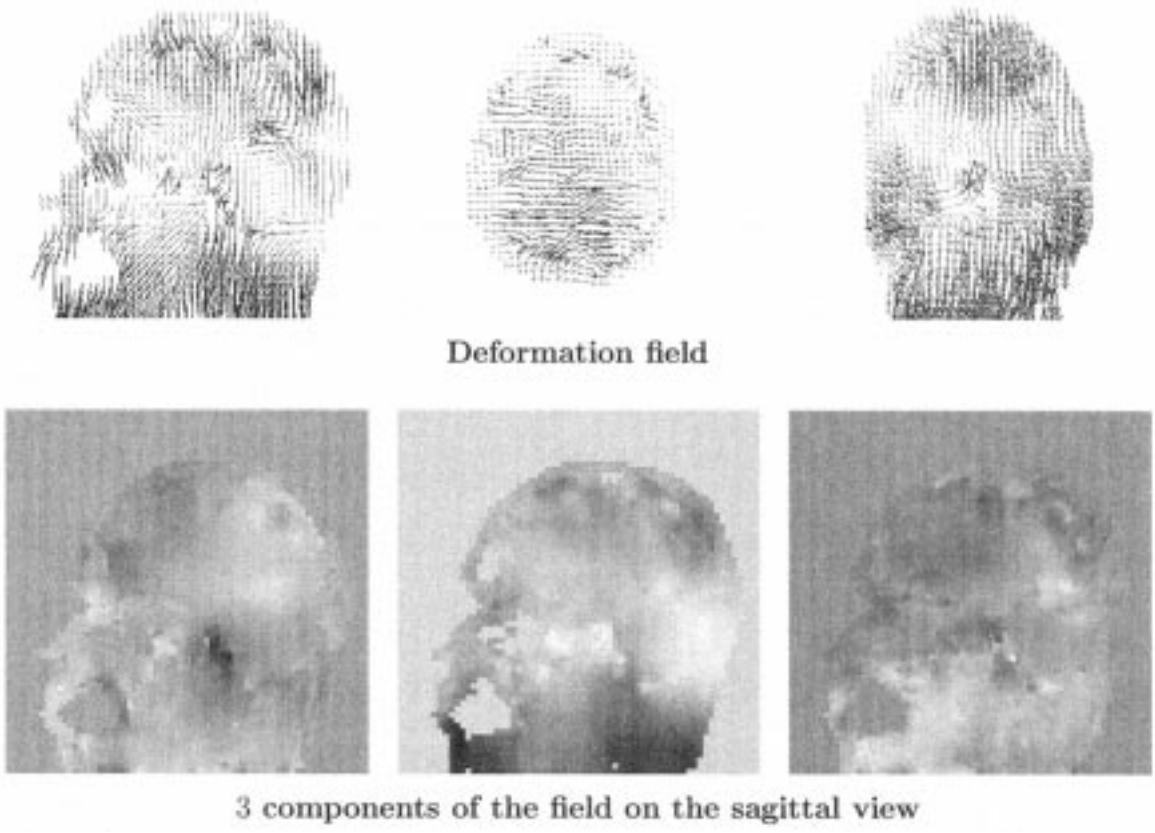

Fig. 11. Top: deformation field. Bottom: Images of the three components of the field on the sagittal view. The 3-D deformation field is subsampled in order to be easier to look at. Although discontinuities are visible, the general spatial coherence of the final deformation field is visible, due to the regularization. The field also confirms that there is no "block-effect" in the registration process.

show the three components of the field on the sagittal view. Although discontinuities are visible, the general spatial coherence of the final deformation field is visible, due to the regularization. The field also confirms that there is no "block-effect" in the registration process.

The computation takes about one-and-one-half hours on a Sun Ultra Sparc 30 (300-MHz) workstation. The volumes are $256 \times 256 \times 200$. We use three levels of resolution ($k = 0$, 1, 2) because the displacement amplitude may reach 30 voxels, and at each resolution level we perform the registration from grid level 4 until grid level 0.

C. Experiments on a Dataset of 18 Subjects

To validate the registration method on a larger database, we acquired MRI-T1 volumetric data of 18 patients. One subject was chosen as the reference subject. We then perform the registration between the reference volume (source) and each of the other subjects (target) *always* using the same set of parameters for the algorithm. Finally, we obtained 17 reconstructed volumes that can be compared to the reference volume. We averaged all the reconstructed volume in order to have a global overview of the quality of the method.

1) Average Deformed Volume: Figs. 12 and 13 present the averaging between 17 patients after a global affine registration (top), after a quadratic multigrid registration, i.e., the method without robust estimators (middle), and the average volume after a robust multigrid registration (bottom). After global affine registration and averaging, we notice that the internal anatomical structures are blurred, because the registration is not precise enough. However, after a robust multigrid registration, we may distinguish precisely the contours of anatomical structures, such as ventricles, deep nuclei, white matter tracks, and even cortical regions (sylvian fissure and parietal region for instance).

The comparison between the quadratic registration and the robust registration shows the benefit of robust functions, because cortical regions are better registered. The mse between the reference volume and the averaged volume is 892 for quadratic registration, and drops to 584 for robust registration. We must note that, considering two subjects, the mse is not a good absolute measure of the quality of the registration because of the acquisition (a simple translation between the two histogram can lead to large mse). However, the mse is a good relative measure to compare two registration processes over a large database.

This experiments clearly show the significant impact of robust estimators. All the more, it validates the assumption that it is necessary to let discontinuities appear in the deformation field to register brains correctly. These experiments also demonstrate the robustness of the method (robustness with respect to the acquisitions and also with respect to the algorithm parameters) over a realistic database of subjects.

2) Overlapping of Brain Tissues: The evaluation must not be based only on a measure that is more or less related to the

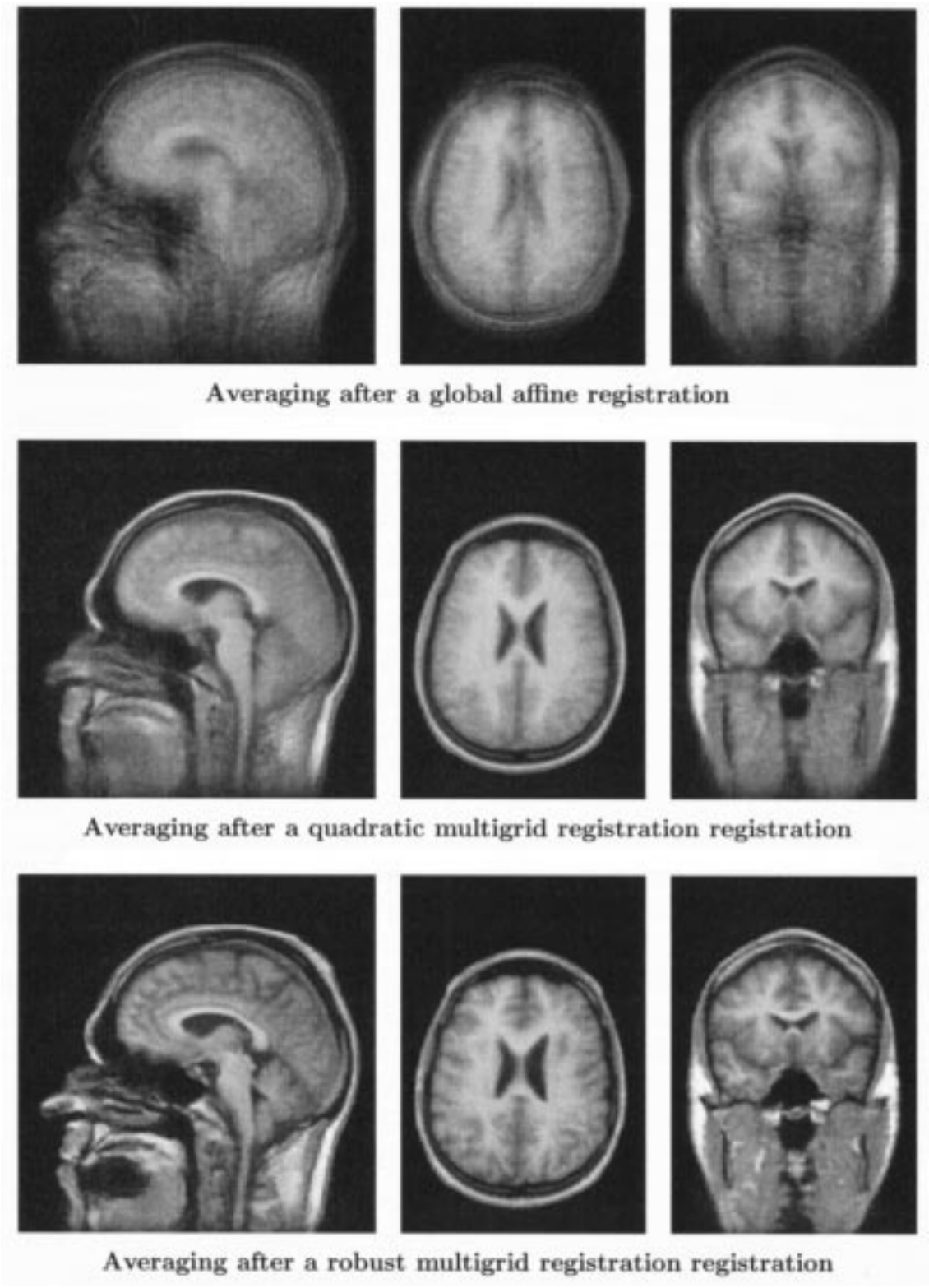

Fig. 12. Results of experiments on a database of 18 subjects. One subject was chosen as the reference subject (see Fig. 13), and we averaged all the reconstructed volumes after global affine registration (top), after quadratic multigrid registration (middle) and after robust multigrid registration (bottom). We kept the same set of parameters for all the subjects. This demonstrate the robustness of the method, and the importance of robust estimators (the quadratic registration is less accurate on the cortex).

image similarity. Therefore, as in Section III-A1, we evaluate in this section the registration process by computing the overlap between the tissues (grey matter and white matter) of the reference volumes and the tissues of each studied volume after registration. We measure the overlap with the total performance, which has already been presented in Section III-A1.

The extraction of grey matter and white matter is performed using a technique presented in [34]. It consists in a 3-D texture

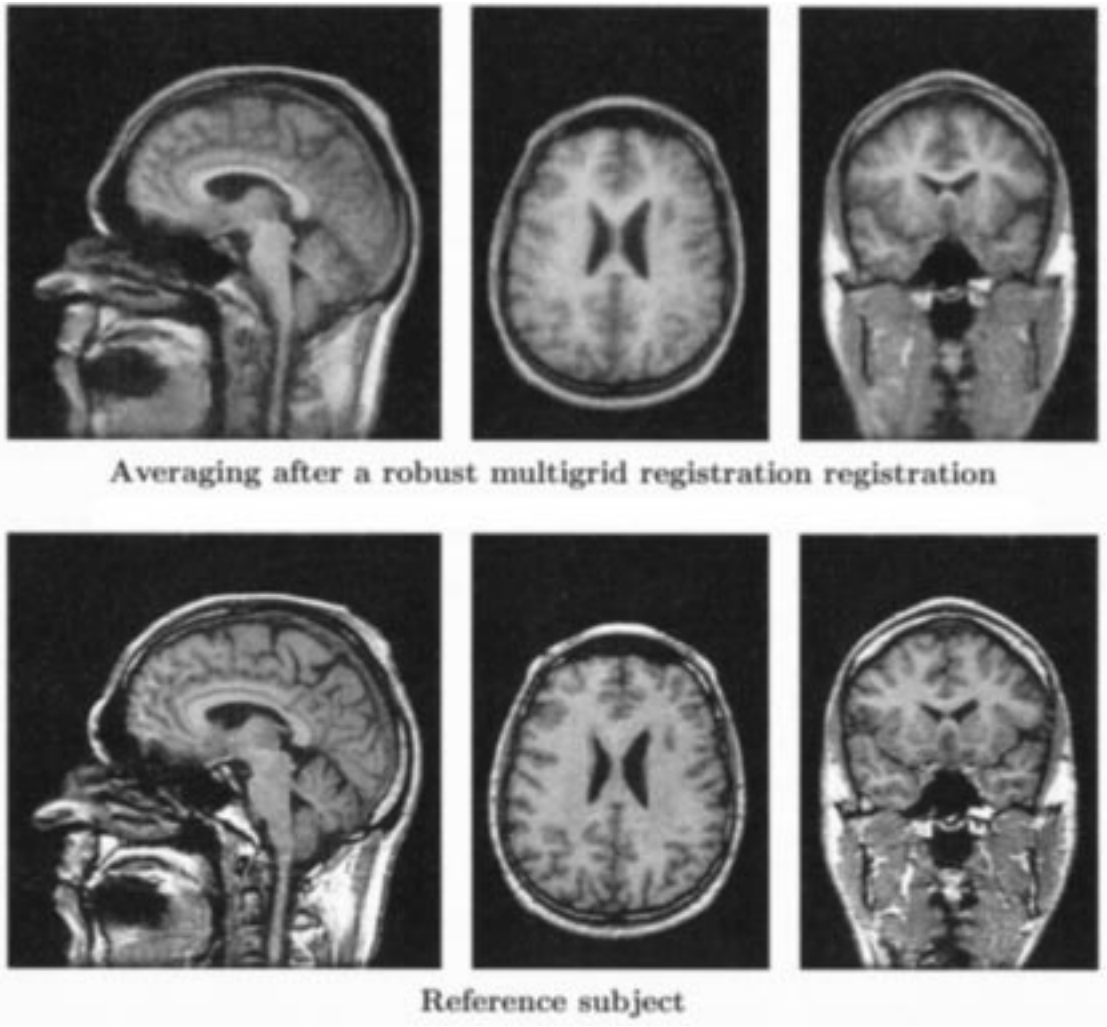

Fig. 13. Results of experiments on a database of 18 subjects. One subject was chosen as the reference subject (bottom), and we averaged all the reconstructed volumes after robust multigrid registration (top). We kept the same set of parameters for all the subjects, which demonstrates the robustness of the method. Results of the averaging after registration show the accuracy of the registration (after averaging we can distinguish precisely anatomical structures such as ventricles, deep nuclei, white matter tracks and even cortical regions).

analysis to compute statistical attributes of each voxels. A clustering procedure is used to find the initial discrimination of the data, and a bayesian relaxation refines the primary decision.

For grey matter tissue, the average overlap after registration is 93.9% (mean of total performance). For white matter, the average overlap is 94.9%. If we perform a rigid registration by maximization of mutual information, we obtain 88.3% and 87.1% of average overlap, for grey matter and white matter respectively. These measures must be interpreted carefully for two reasons. We use binary classes (and not fuzzy classes) and a simple trilinear interpolation scheme, which may introduce some error. Furthermore, the classification algorithm introduces errors that disturb the overlap measure. In the last 5% to recover, it is difficult to distinguish what is due to the registration process and what is due to interpolation and segmentation errors. However, these overlap measures show the benefit of non rigid registration.

IV. Conclusion

We have presented in this paper a new registration method based on a dense robust 3-D estimation of the optical flow with a piecewise parametric description of the deformation field. The performance of this method was evaluated objectively on simulated data and results are presented on different real data, demonstrating the significant impact of the method. We show that the method is robust with respect to the parameters, as well as with respect to the differences of acquisition of MRI scans. We also show the benefits of robust estimators on a large database of subjects.

We use an efficient minimization framework, both multiresolution and multigrid with robust estimators. This optimization scheme is not limited to the estimation of the optical flow, but may as well be adapted to other similarity measures, leading to different registration applications. The adaptive partition of the volume accelerates the algorithm and improves the estimation in the regions of interest.

In the future, we intend to investigate the integration of cortical features [35] in the registration process. Some interesting work [20], [19], [53] has already been done in that direction, and we think that the energy based framework that we have presented, coupled with the adaptive multigrid minimization, is

naturally adapted to cooperation between luminance based registration and local approaches.

REFERENCES

[1] R. Bajcsy and S. Kovacic, "Multiresolution elastic matching," *Comput. Vis., Graph., Image Processing*, vol. 46, pp. 1–21, 1989.

[2] C. Barillot, B. Gibaud, J. C. Gee, and D. Lemoine, "Segmentation and fusion of multimodality and multi-subjects data for the preparation of neurosurgical procedures," in *Medical Imaging: Analysis of Multimodality 2D/3D Images*, L. Beolchi and M. H. Kuhn, Eds. Amsterdam, The Netherlands: IOS, 1995, vol. 19, pp. 70–82.

[3] J. Barron, D. Fleet, S. Beauchemin, and T. Burkitt, "Performance of optical flow techniques," in *Proc. Conf. Computer Vision Pattern Recognition*, Champaign, IL, June 1992, pp. 236–242.

[4] R. Battiti, E. Amaldi, and C. Koch, "Computing optical flow over multiple scales: An adaptive coarse-to-fine strategy," *Int. J. Comput. Vis.*, vol. 6, no. 2, pp. 133–146, 1991.

[5] S. Beauchemin and J. Barron, "The computation of optical flow," *ACM Computing Surveys*, vol. 27, no. 3, pp. 433–467, 1995.

[6] J. Bergen, P. Anadan, K. Hanna, and R. Hingorani, "Hierarchical model-based motion estimation," in *Proc. Eur. Conf. Computer Vision*, 1991, pp. 5–10.

[7] M. Black and P. Anandan, "The robust estimation of multiple motions: Parametric and piecewise-smooth flow fields," *Computer Vision and Image Understanding*, vol. 63, no. 1, pp. 75–104, 1996.

[8] M. Black and A. Rangarajan, "On the unification of line processes, outlier rejection, and robust statistics with application in early vision," *Int. J. Comput. Vision*, vol. 19, no. 1, pp. 57–91, 1996.

[9] F. Bookstein, "Principal warps: Thin plate splines and the decomposition of deformations," *IEEE Trans. Pattern Anal. Machine Intell.*, vol. 11, pp. 567–585, June 1989.

[10] M. Bro-Nielsen and C. Gramkow, "Fast fluid registration of medical images," in *Proc. Visualization in Biomedical Computing*, K. H. Hohne and R. Kikinis, Eds., Sept. 1996, pp. 267–276. No. 1131 in Lecture Notes in Computer Science.

[11] J. P. Burt, "The pyramide as a structure for efficient computation," in *Multiresolution Image Processing and Analysis*, ser. Information Science. Berlin, Germany: Springer-verlag, 1984, ch. 12, pp. 6–38.

[12] P. Charbonnier, L. Blanc-Féraud, G. Aubert, and M. Barlaud, "Deterministic edge preserving regularization in computed imaging," *IEEE Trans. Image Processing*, vol. 6, pp. 298–311, Feb 1997.

[13] G. Christensen, "Consistent linear-elastic transformations for image matching," in *Proc. Information Processing in Medical Imaging*, June 1999, pp. 224–237. No. 1613 in Lecture Notes in Computer Science.

[14] G. Christensen, R. Rabbit, and M. I. Miller, "Deformable templates using large deformation kinematics," *IEEE Trans. Image Processing*, vol. 5, pp. 1435–1447, Oct. 1996.

[15] I. Cohen and I. Herlin, "Optical flow and phase portrait methods for environmental satellite image sequences," in *Proc. Eur. Conf. Computer Vision*, Cambridge, UK, Apr. 1996, pp. II:141–150.

[16] L. Cohen and I. Cohen, "Finite element method for active contour models and ballons for 2-D and 3-D images," *IEEE Trans. Pattern Anal. Machine Intell.*, vol. 15, pp. 1131–1147, Nov. 1993.

[17] D. L. Collins, A. P. Zijdenbos, V. Kollokian, J. G. Sled, N. J. Kabani, C. J. Holmes, and A. C. Evans, "Design and construction of a realistic digital brain phantom," *IEEE Trans. Med. Imag.*, vol. 17, pp. 463–468, June 1998.

[18] L. Collins and A. Evans, "Animal: Validation and applications of nonlinear registration-based segmentation," *Int. J. Pattern Recogn. Artif. Intell.*, vol. 8, no. 11, pp. 1271–1294, 1997.

[19] L. Collins, G. Le Goualher, and A. Evans, "Non linear cerebral registration with sulcal constraints," in *Proc. Medical Image Computing and Computer-Assisted Intervention*, A. Colchester and S. Delp, Eds, Oct. 1998, pp. 974–985. No. 1496 in Lecture Notes in Computer Science.

[20] L. Collins, G. Le Goualher, R. Venugopal, A. Caramanos, A. Evans, and C. Barillot, "Cortical constraints for nonlinear cortical registration," in *Proc. Visualization in Biomedical Computing*, K. H. Hohne and R. Kikinis, Eds, Sept. 1996, pp. 307–316. No. 1131 in Lecture Notes in Computer Science.

[21] C. Davatzikos, "Spatial transformation and registration of brain images using elastically deformable models," *Comput. Vis. Image Understanding*, vol. 66, no. 2, pp. 207–222, 1997.

[22] A. Delaney and Y. Bresler, "Globally convergent edge-preserving regularized reconstruction: An application to limited-angle tomography," *IEEE Trans. Image Processing*, vol. 7, pp. 204–221, Feb. 1998.

[23] R. Deriche. (1993, Apr.) Recursively Implementing the Gaussian and Its Derivatives. INRIA. [Online]. Available: http://www.inria.fr/RRRT/RR-1893.html

[24] W. Enkelmann, "Investigations of multigrid algorithms for the estimation of optical flow fields in image sequences," *Comput. Vis., Graph., Image Processing*, vol. 43, no. 2, pp. 150–177, 1988.

[25] A. C. Evans, W. Dai, D. L. Collins, P. Neelin, and T. Marrett, "Warping of computerized 3-D atlas to match brain image volumes for quantitative neuroanatomical and functionnal analysis," presented at the Int. Soc. Optical Engineering: Medical Imaging V, 1991.

[26] J. C. Gee, M. Reivicj, and R. Bajcsy, "Elastically deforming 3-D atlas to match anatomical brain images," *J. Comput. Assist. Tomogr.*, vol. 17, no. 2, pp. 225–236, 1993.

[27] B. Gibaud, S. Garlatti, C. Barillot, and E. Faure, "Computerised brain atlases vs. decision support systems: A methodological approach," *Artif. Intell. Med.*, vol. 14, no. 1, pp. 83–100, 1998.

[28] W. Hackbusch, *Multigrid Methods and Applications*. Berlin, Germany: Springer Verlag, 1985.

[29] P. Hellier, C. Barillot, E. Mémin, and P. Pérez, "Medical image registration with robust multigrid techniques," in *Proc. Medical Image Computing and Computer-Assisted Intervention*, C. Taylor and A. Colchester, Eds., Sept. 1999, pp. 680–687. No. 1679 in Lecture Notes in Computer Science.

[30] ——, "An energy-based framework for dense 3-D registration of volumetric brain image," in *IEEE Conf. Computer Vision and Pattern Recognition*, vol. II, Hilton Head Island, SC, June 2000, pp. 270–275.

[31] B. Horn and B. Schunck, "Determining optical flow," *Artif. Intell.*, vol. 17, pp. 185–203, Aug. 1981.

[32] P. Huber, *Robust Statistics*. New York: Wiley, 1981.

[33] J. Konrad and E. Dubois, "Bayesian estimation of motion vector fields," *IEEE Trans. Pattern Anal. Machine Intell.*, vol. 14, pp. 910–927, Sept. 1992.

[34] F. Lachmann and C. Barillot, "Brain tissue classification from MRI data by means of texture analysis," in *Proc. Medical Imaging VI: Image Processing*, vol. 1652, 1992, pp. 72–83.

[35] G. Le Goualher, C. Barillot, and Y. Bizais, "Modeling cortical sulci with active ribbons," *Int. J. Pattern Recogn. Artif. Intell.*, vol. 8, no. 11, pp. 1295–1315, 1997.

[36] J. Maintz and M. A. Viergever, "A survey of medical image registration," *Med. Image Anal.*, vol. 2, no. 1, pp. 1–36, 1998.

[37] C. R. Maurer and J. M. Fitzpatrick, "A review of medical image registration," in *Interactive Image Guided Neurosurgery*. Las Vegas, NV: Amer. Assoc. Neurological Surgeons, 1993, pp. 17–44.

[38] S. McCormick, *Multilevel Adaptive Methods for Partial Differential Equations*. Philadelphia, PA: SIAM, 1989.

[39] E. Mémin and P. Pérez, "Dense estimation and object-based segmentation of the optical flow with robust techniques," *IEEE Trans. Image Processing*, vol. 7, pp. 703–719, May 1998.

[40] ——, "A multigrid approach for hierarchical motion estimation," in *Proc. Int. Conf. Computer Vision*, Bombay, Maharashtra, India, Jan. 1998, pp. 933–938.

[41] E. Mémin and T. Risset. (2000) VlSI design methodology for edge-preserving image reconstruction. *Real-Time Imag.* [Online]. Available: http://www.irisa.fr/EXTERNE/bibli/pi/1220/1220.html

[42] O. Musse, F. Heitz, and J. P. Armspach, "3-D deformable image matching using multiscale minimization of global energy functions," in *Proc. Conf. Computer Vision Pattern Recognition*, vol. 2, Fort Collins, CO, June 1999, pp. 478–485.

[43] J. M. Odobez and P. Bouthemy, "Robust multiresolution estimation of parametric motion models," *J. Visual Commun. Image Representation*, vol. 6, no. 4, pp. 348–365, 1995.

[44] M. Ono, S. Kubik, and C. Abernathey, *Atlas of the Cerebral Sulci*. Berlin, Germany: Springer-Verlag, 1990.

[45] X. Pennec, P. Cachier, and N. Ayache, "Understanding the demon's algorithm: 3-D non rigid registration by gradient descent," in *Proc. Medical Image Computing and Computer-Assisted Intervention*, C. Taylor and A. Colchester, Eds., Sept. 1999, pp. 597–605. No. 1679 in Lecture Notes in Computer Science.

[46] C. Schnörr, "A study of convex variational diffusion approach for image segmentation and feature extraction," *J. Math. Imag. Vis.*, vol. 8, no. 3, pp. 271–292, 1998.

[47] G. Subsol, J. P. Thirion, and N. Ayache, "A general scheme for automatically building 3-D morphometric anatomical atlases: Application to a skull atlas," *Med. Image Anal.*, vol. 2, no. 1, pp. 37–60, 1998.

[48] R. Szeliski and S. Lavallée, "Matching 3-D anatomical surfaces with nonrigid deformations using octree-splines," *SPIE Geometric Meth. Comput. Vis.*, vol. 2031, pp. 306–315, 1993.

[49] J. Talairach and P. Tournoux, *Co-Planar Stereotaxic Atlas of the Human Brain*, Stuttgart, Germany: Georg Thieme Verlag, 1988.

[50] D. Terzopoulos, "Image analysis using multigrid relaxation methods," *IEEE Trans. Pattern Anal. Machine Intell.*, vol. PAMI-8, pp. 129–139, Feb. 1986.

[51] J. P. Thirion, "Image matching as a diffusion process: An analogy with Maxwell's demons," *Med. Image Anal.*, vol. 2, no. 3, pp. 243–260, 1998.

[52] P. Thompson and A. Toga, "A surface-based technique for warping three-dimensional images of the brain," *IEEE Trans. Med. Imag.*, vol. 15, pp. 402–417, Aug. 1996.

[53] M. Vaillant and C. Davatzikos, "Hierarchical matching of cortical features for deformable brain image registration," in *Proc. Information Processing in Medical Imaging*, June 1999, pp. 182–195. No. 1613 in Lecture Notes in Computer SCience.

[54] J. H. Van Bemmel and M. A. Musen. (1997) Handbook of Medical Informatics. Springer-Verlag, Berlin, Germany. [Online]. Available: http://www.mieur.nl/mihandbook

[55] P. A. Van den Elsen, E. D. Pol, and M. A. Viergever, "Medical image matching: A review with classification," *IEEE Eng. Med. Biol. Mag.*, vol. 12, pp. 26–38, 1993.